Nuclear reaction studies of unstable nuclei using relativistic mean field formalisms in conjunction with the Glauber model

A. Shukla,[1,2] B. K. Sharma,[1] R. Chandra,[1] P. Arumugam,[3] and S. K. Patra[1]

[1]*Institute of Physics, Sachivalaya Marg, Bhubaneswar-751005, India*

[2]*Department of Physics and Astronomy, University of North Carolina, Chapel Hill, North Carolina 27599, USA*

[3]*Centro de Física das Interacções Fundamentais, and Departmento de Física, Instituto Superior Técnico, Avenida Rovisco Pais, P1049-001 Lisbon, Portugal*

(Received 22 March 2007; published 4 September 2007)

We study nuclear reaction cross sections for stable and unstable projectiles and targets within Glauber model, using densities obtained from various relativistic mean-field formalisms. The calculated cross sections are compared with the experimental data in some specific cases. We also evaluate the differential scattering cross sections at several incident energies and observe that the results found from various densities are similar at smaller scattering angles, whereas a systematic deviation is noticed at large angles. In general, these results agree fairly well with the experimental data.

DOI: 10.1103/PhysRevC.76.034601 PACS number(s): 21.10.Ft, 21.30.−x, 24.10.Jv, 25.60.−t

I. INTRODUCTION

Study of unstable nuclei with radioactive ion-beam (RIB) facilities has opened an exciting channel to look for some crucial issues in context of both nuclear structure and nuclear astrophysics [1–3]. Unstable nuclei play an influential, and in some cases dominant, role in many phenomena in the cosmos such as novae, supernovae, X-ray bursts, and other stellar explosions. At extremely high temperatures ($>10^8$ K) of these astrophysical environments, the interaction times between nuclei can be so short (∼seconds) that unstable nuclei formed in a nuclear reaction can undergo subsequent reactions before they decay. Sequences of (predominantly unmeasured) nuclear reactions occurring in exploding stars are therefore quite different than sequences occurring at lower temperatures, for example, characteristic of those occurring in Sun. The direct study of stellar properties in ground-based laboratories has become more attractive, due to the availability of RIBs, for example, the study of ^{18}Ne-induced neutron pickup reactions could reveal information about the exotic ^{15}O+^{19}Ne reaction happening in the CNO cycle in burning stars. Study of the structure and reactions of unstable nuclei is therefore required to improve our understanding of the astrophysical origin of atomic nuclei and the evolution of stars and their (sometimes explosive) deaths.

Experimental study of unstable nuclei has considerably advanced through the technique of using secondary radioactive beams. The quantities measured in the study include various inclusive cross sections, for example, reaction or interaction cross sections, nucleon-removal cross sections, Coulomb breakup cross sections and momentum distributions of a fragment. These quantities have played an important role to reveal the nuclear structure of unstable nuclei, particularly halo structure near the drip line [4]. The total reaction cross section (σ_r) is one of the most fundamental quantities characterizing the nuclear reactions and to probe for nuclear structure details. Recent studies using RIB have demonstrated a large enhancement of σ_r induced by neutron-rich nuclei, which has been interpreted as neutron halo [5–8] (such as ^{11}Li, ^{11,14}Be, etc.) and neutron skin structure [8] (such as ^{6}He and ^{8}He). The halo structure of ^{11}Li seems to be consistent with all the experimental results, including the enhancement of interaction cross section σ_I, the enhancement of two-neutron removal cross section (σ_{2n}), and the narrow peak in the momentum distribution of fragmentation of ^{9}Li.

At present the Glauber model is a standard tool to calculate the cross sections because it can account for a significant part of breakup effects that play an important role in the reaction of a weakly bound nucleus [9,10]. The Glauber model, based on the independent individual nucleon-nucleon collisions in the overlap zone of the colliding nuclei [11], has been used extensively to explain the observed nuclear reaction cross section for various systems at high energies [12,13]. This model requires the structure information, namely the density profiles, of the nuclei involved. This information has to be provided by nuclear structure models, like the relativistic mean-field (RMF) theory, which recently has been effectively used for this purpose [14,15].

The RMF formalism is well suited for the studies of exotic nuclei [16]. It takes into account the spin orbit interaction automatically, unlike to the nonrelativistic case. The parameters are fitted by taking into account the properties of few spherical nuclei. The inclusion of ρ meson takes into account the proton-neutron asymmetry and gives an impression that the theory can be used to nuclei far away from the valley of β stability. Apart from these, the advantage of the RMF model is the microscopic calculations of nuclear structure starting from the Lagrangian with same parameters applicable for the whole nuclear chart and beyond. The recent extension of this formalism with field-theory-motivated effective Lagrangian approach (E-RMF) [17,18] could extend the applicability of this model to neutron stars and infinite nuclear matter [19]. Hence this model provides us better predictability to explore the features of exotic nuclei.

The main objective of the present work is to study the nuclear reaction cross section using RMF and E-RMF nuclear densities in conjunction with the Glauber model. The article

is presented as follows. In Sec. II, we discuss in brief the formalism used in the present work. In Sec. III, we discuss our results for the ground-state properties of few selected light mass nuclei and cross sections of reactions involving them. The summary and concluding remarks are given in Sec. IV.

II. FORMALISM

A. E-RMF approach for nuclear structure

The details of the standard RMF formalism for finite nuclei can be found in Refs. [16]. The recent extension of RMF formalism based on the field-theory-motivated effective Lagrangian approach, known as E-RMF, can be found in Refs. [20,21]. The energy-density functional of the E-RMF model for finite nuclei [17,18,20,21] is written as

$$\begin{aligned}\mathcal{E}(\mathbf{r}) = \sum_{\alpha}\varphi_{\alpha}^{\dagger}\Bigg[& -i\boldsymbol{\alpha}\cdot\boldsymbol{\nabla}+\beta(M-\Phi)+W+\frac{1}{2}\tau_3 R \\ & +\frac{1+\tau_3}{2}A-\frac{i}{2M}\beta\boldsymbol{\alpha}\cdot\Bigg(f_v\boldsymbol{\nabla}W+\frac{1}{2}f_\rho\tau_3\boldsymbol{\nabla}R \\ & +\lambda\boldsymbol{\nabla}A\Bigg)+\frac{1}{2M^2}\left(\beta_s+\beta_v\tau_3\right)\Delta A\Bigg]\varphi_{\alpha} \\ & +\left(\frac{1}{2}+\frac{\kappa_3}{3!}\frac{\Phi}{M}+\frac{\kappa_4}{4!}\frac{\Phi^2}{M^2}\right)\frac{m_s^2}{g_s^2}\Phi^2-\frac{\zeta_0}{4!}\frac{1}{g_v^2}W^4 \\ & +\frac{1}{2g_s^2}\left(1+\alpha_1\frac{\Phi}{M}\right)(\boldsymbol{\nabla}\Phi)^2-\frac{1}{2g_v^2}\left(1+\alpha_2\frac{\Phi}{M}\right) \\ & \times(\boldsymbol{\nabla}W)^2-\frac{1}{2}\left(1+\eta_1\frac{\Phi}{M}+\frac{\eta_2}{2}\frac{\Phi^2}{M^2}\right)\frac{{m_v}^2}{{g_v}^2}W^2 \\ & -\frac{1}{2g_\rho^2}(\boldsymbol{\nabla}R)^2-\frac{1}{2}\left(1+\eta_\rho\frac{\Phi}{M}\right)\frac{m_\rho^2}{g_\rho^2}R^2 \\ & -\frac{1}{2e^2}(\boldsymbol{\nabla}A)^2+\frac{1}{3g_\gamma g_v}A\Delta W+\frac{1}{g_\gamma g_\rho}A\Delta R, \end{aligned} \tag{1}$$

where the index α runs over all occupied states $\varphi_\alpha(\mathbf{r})$ of the positive-energy spectrum, $\Phi \equiv g_s\phi_0(\mathbf{r})$, $W \equiv g_v V_0(\mathbf{r})$, $R \equiv g_\rho b_0(\mathbf{r})$, and $A \equiv eA_0(\mathbf{r})$.

The terms with g_γ, λ, β_s, and β_v take care of effects related with the electromagnetic structure of the pion and the nucleon (see Ref. [18]). Specifically, the constant g_γ concerns the coupling of the photon to the pions and the nucleons through the exchange of neutral vector mesons. The experimental value is $g_\gamma^2/4\pi = 2.0$. The constant λ is needed to reproduce the magnetic moments of the nucleons. It is defined by

$$\lambda = \tfrac{1}{2}\lambda_p(1+\tau_3)+\tfrac{1}{2}\lambda_n(1-\tau_3), \tag{2}$$

with $\lambda_p = 1.793$ and $\lambda_n = -1.913$ the anomalous magnetic moments of the proton and the neutron, respectively. The terms with β_s and β_v contribute to the charge radii of the nucleon [18].

The energy density contains tensor couplings and scalar-vector and vector-vector meson interactions in addition to the standard scalar self-interactions κ_3 and κ_4. The E-RMF formalism can be interpreted as a covariant formulation of density functional theory as it contains all the higher-order terms in the Lagrangian by expanding it in powers of the meson fields. The terms in the Lagrangian are kept finite by adjusting the parameters. Further insight into the concepts of the E-RMF model can be obtained from Ref. [18]. It is worth mentioning that the standard RMF Lagrangian is obtained by ignoring the vector-vector and scalar-vector cross interactions and needs no separate discussion. The field equations and numerical details can be obtained in Refs. [16,20,21]. The set of coupled equations is solved numerically by a self-consistent iteration method. The baryon, scalar, isovector, proton, and tensor densities are

$$\rho(r) = \sum_{\alpha}\varphi_{\alpha}^{\dagger}(r)\varphi_{\alpha}(r), \tag{3}$$

$$\rho_s(r) = \sum_{\alpha}\varphi_{\alpha}^{\dagger}(r)\beta\varphi_{\alpha}(r), \tag{4}$$

$$\rho_3(r) = \sum_{\alpha}\varphi_{\alpha}^{\dagger}(r)\tau_3\varphi_{\alpha}(r), \tag{5}$$

$$\rho_{\mathrm{p}}(r) = \sum_{\alpha}\varphi_{\alpha}^{\dagger}(r)\left(\frac{1+\tau_3}{2}\right)\varphi_{\alpha}(r), \tag{6}$$

$$\rho_{\mathrm{T}}(r) = \sum_{\alpha}\frac{i}{M}\boldsymbol{\nabla}\cdot[\varphi_{\alpha}^{\dagger}(r)\beta\boldsymbol{\alpha}\varphi_{\alpha}(r)], \tag{7}$$

$$\rho_{\mathrm{T},3}(r) = \sum_{\alpha}\frac{i}{M}\boldsymbol{\nabla}\cdot[\varphi_{\alpha}^{\dagger}(r)\beta\boldsymbol{\alpha}\tau_3\varphi_{\alpha}(r)]. \tag{8}$$

For the calculation of ground-state properties of finite nuclei, we refer the readers to Refs. [16,20,21].

B. Glauber model for nuclear reactions

The theoretical formalism to calculate the nuclear reaction cross section using Glauber approach has been given by R. J. Glauber [11]. For sake of completeness, here, we briefly outline the steps of derivations following the notation of Ref. [11].

The standard Glauber form for the reaction cross section at high energies, is expressed [11] as:

$$\sigma_R = 2\pi\int_0^{\infty} b[1-T(b)]db, \tag{9}$$

where $T(b)$, the transparency function, is the probability that at an impact parameter b the projectile pass through the target without interacting. This function $T(b)$ is calculated in the overlap region between the projectile and target where the interactions are assumed to result from single nucleon-nucleon collision and is given by

$$T(b) = \exp\left[-\sum_{i,j}\overline{\sigma}_{ij}\int d\vec{s}\,\overline{\rho}_{ti}(s)\,\overline{\rho}_{pj}(|\vec{b}-\vec{s}|s)\right]. \tag{10}$$

Here, the summation indices i, j run over proton and neutron and subscript p and t refers to projectile and target, respectively. $\overline{\sigma}_{ij}$ is the experimental nucleon-nucleon reaction cross-section that varies with respect to energy. The z-integrated densities $\overline{\rho}(\omega)$ are defined as

$$\overline{\rho}(\omega) = \int_{-\infty}^{\infty}\rho\left(\sqrt{\omega^2+z^2}\right)dz, \tag{11}$$

with $\omega^2 = x^2 + y^2$. The parameters σ_{NN}, α, and β usually depend on either the proton-proton (neutron-neutron) or proton-neutron case, but we have used some appropriate average values in the present calculations [22]. The argument of $T(b)$ in Eq. (10) is $|\vec{b} - \vec{s}|$, which stands for the impact parameter between ith and jth nucleons.

The Glauber model agrees very well with the experimental data at high energies. However, this model fails to describe, reasonably, the collisions induced at relatively low energies. In such a case the present version of the Glauber model is modified to take care of finite range effects in profile functions and Coulomb modified trajectories. Thus for finite range approximations, the transparency function is given by

$$T(b) = \exp\left\{-\int_p \int_t \sum_{i,j} [\Gamma_{ij}(\vec{b} - \vec{s} + \vec{t})]\overline{\rho}_{pi}(\vec{t})\overline{\rho}_{tj}(\vec{s})\, d\vec{s} d\vec{t}\right\}. \tag{12}$$

Here the profile function Γ_{ij} is given by

$$\Gamma_{ij}(b_{\text{eff}}) = \frac{1 - i\alpha}{2\pi\beta_{NN}^2}\bar{\sigma}_{ij} \exp\left(-\frac{b_{\text{eff}}^2}{2\beta_{NN}^2}\right), \tag{13}$$

where $b_{\text{eff}} = |\vec{b} - \vec{s} + \vec{t}|$, $\vec{b}$ is the impact parameter and $\vec{s}$ and $\vec{t}$ are just the dummy variables for integration over the z-integrated target and projectile densities.

1. Differential cross section

The differential elastic cross section by the ratio to the Rutherford cross section is given by

$$\frac{d\sigma}{d\Omega} = \frac{|F(q)|^2}{|F_{\text{coul}}(q)|^2}. \tag{14}$$

$F(q)$ and $F_{\text{coul}}(q)$ are the elastic and Coulomb (elastic) scattering amplitudes, respectively.

The elastic scattering amplitude $F(q)$ is written as

$$F(q) = e^{i\chi_s}\left\{F_{\text{coul}}(q) + \frac{iK}{2\pi}\int db \exp[-i\vec{q}\cdot\vec{b} + 2i\eta \ln(Kb)]T(b)\right\} \tag{15}$$

with the Coulomb elastic scattering amplitude $F_{\text{coul}}(q)$ given by

$$F_{\text{coul}}(q) = \frac{-2\eta K}{q^2}\exp\left[-2i\eta \ln\left(\frac{q}{2K}\right) + 2i \arg\Gamma(1 + i\eta)\right]. \tag{16}$$

Here $\eta = Z_P Z_T e^2/\hbar v$ is the Sommerfield parameter, v is the incident velocity, and $\chi_s = -2\eta \ln(2Ka)$ with a being screening radius [11]. The elastic differential cross section does not depend on the screening radius a.

III. RESULTS AND DISCUSSION

A. Ground-state properties from RMF models

There exist a number of parameter sets for solving the standard RMF as well as E-RMF Lagrangians. In our previous article [15] we calculated reaction cross sections with densities obtained from various interactions. In the present work, we employ the SIG-OM set for RMF that was recently used by Haidari *et al.* [23] and G2 [20] for E-RMF calculations.

TABLE I. The ground-state properties of the nuclei involved in the reaction cross-section study. Experimental binding energies were taken from Ref. [24]. The SIG-OM and G2 sets are chosen for RMF and E-RMF parametrizations, respectively.

Nuclei	Charge radii (in fm)			Binding energy (in MeV)		
	RMF	E-RMF	Expt. [25]	RMF	E-RMF	Expt. [24]
^{12}C	2.466	2.497	2.470	84.061	87.230	92.162
^{6}Li	2.525	2.512	2.539	29.377	31.936	31.994
^{7}Li	2.363	2.354	2.431	33.444	36.538	39.244
^{8}Li	2.281	2.264		38.664	42.214	41.277
^{9}Li	2.234	2.202		44.825	48.761	45.341
^{10}Li	2.261	2.230		47.168	50.937	45.316
^{11}Li	2.291	2.266		50.453	53.997	45.640
^{7}Be	2.685	2.680		31.736	34.862	37.600
^{8}Be	2.497	2.504		39.146	42.706	56.500
^{9}Be	2.401	2.405	2.518	47.805	51.620	58.165
^{10}Be	2.341	2.336		57.328	61.265	64.977
^{11}Be	2.368	2.367		61.911	65.627	65.481
^{12}Be	2.393	2.397		67.341	70.735	68.650
^{13}Be	2.411	2.406		64.982	69.109	68.549
^{14}Be	2.428	2.412		63.097	67.892	69.916
^{8}B	2.769	2.776		34.718	38.359	37.737
^{9}B	2.578	2.598		45.502	49.392	56.314
^{10}B	2.472	2.492	2.428	57.556	61.420	64.751
^{11}B	2.412	2.428	2.406	70.562	74.213	76.205
^{12}B	2.434	2.453		77.411	80.784	79.575
^{13}B	2.456	2.478		85.090	88.027	84.453
^{14}B	2.469	2.479		84.044	87.841	85.422
^{15}B	2.482	2.478		83.490	88.098	88.185
^{16}B	2.495	2.477		83.623	88.795	88.144
^{17}B	2.509	2.476		83.976	89.925	89.522

1. Binding energies

We have presented the calculated binding energy using RMF and E-RMF theories in Table I. The experimental data taken from Ref. [24] have also been given for comparison. It is evident from Table II that both the calculated binding energies are similar and slightly overestimate in comparison with experimental binding energies. However, these differences with experimental values are small and may be attributed to the fact that for light mass region of the periodic table, mean field is not saturated. To get a qualitative estimation of the binding energy, the RMF as well as E-RMF results are trustworthy and can be used for further calculations in this region.

2. Nuclear radii

The root-mean-square (rms) charge radius (r_c) is obtained from the point proton rms radius through the relation given

TABLE II. The coefficients of Gaussian functions fitted to mimic the density distributions from RMF with SIG-OM and E-RMF with G2 parameter sets. The first line corresponds to SIG-OM and the second line to G2 parametrizations.

Nuclei	c_1	a_1	c_2	a_2
^{12}C	−1.19290	0.43150	1.41910	0.36777
	−3.77056	0.37809	3.96943	0.36006
^{6}Li	−1.19320	0.35724	1.42228	0.35709
	−1.20692	0.39464	1.39716	0.38081
^{7}Li	−1.18917	0.31651	1.41291	0.31651
	−0.02297	0.90405	0.20935	0.29855
^{8}Li	−1.18507	0.36369	1.40981	0.34895
	−0.04539	0.70103	0.23248	0.28682
^{9}Li	−0.02607	0.92972	0.24542	0.28133
	−0.07409	0.60134	0.26200	0.27935
^{10}Li	−0.03526	0.79222	0.23711	0.25465
	−0.07966	0.56516	0.25466	0.25458
^{11}Li	−0.05229	0.67219	0.23641	0.23543
	−0.09683	0.51846	0.25806	0.23719
^{7}Be	−1.19498	0.31920	1.41997	0.31896
	−0.01977	0.96010	0.20625	0.29648
^{8}Be	−0.02025	0.98637	0.24419	0.30083
	−0.07016	0.61682	0.25782	0.29849
^{9}Be	−0.06240	0.69377	0.28340	0.30012
	−0.17128	0.49902	0.36183	0.30951
^{10}Be	−0.12156	0.59723	0.34318	0.30291
	−0.40674	0.43037	0.59982	0.32511
^{11}Be	−0.15051	0.54021	0.35239	0.28195
	−0.39959	0.40983	0.57775	0.30105
^{12}Be	−0.19523	0.49296	0.37849	0.26865
	−0.47247	0.38545	0.63604	0.28738
^{13}Be	−0.14949	0.52383	0.33391	0.24652
	−0.25171	0.42035	0.41548	0.25339
^{14}Be	−0.12420	0.54603	0.30791	0.22839
	−0.19132	0.43615	0.353435	0.23129
^{8}B	−1.05597	0.34652	1.28006	0.33463
	−0.03535	0.75948	0.22188	0.28100
^{9}B	−0.05555	0.71516	0.27596	0.29664
	−0.14934	0.51161	0.33920	0.30400
^{10}B	−0.16001	0.56271	0.38264	0.31404
	−1.21376	0.39463	1.40784	0.35375
^{11}B	−0.32664	0.49989	0.55114	0.33064
	−2.79365	0.38139	2.99014	0.36013
^{12}B	−0.49301	0.44359	0.69585	0.32118
	−3.12130	0.36071	3.30124	0.34123
^{13}B	−0.77107	0.40334	0.95417	0.31709
	−3.56218	0.34485	3.72662	0.32706
^{14}B	−0.38333	0.43538	0.56403	0.27802
	−2.54155	0.33298	2.70540	0.30913
^{15}B	−0.29069	0.44877	0.46814	0.25388
	−0.99177	0.33718	1.15357	0.28066
^{16}B	−0.24920	0.45530	0.42450	0.23682
	−0.55398	0.34711	0.71249	0.25353
^{17}B	−0.22619	0.45154	0.39655	0.22176
	−0.43556	0.34777	0.59030	0.23519

below [16]:

$$r_c = \sqrt{r_p^2 + 0.64},$$

considering the size of proton radius as 0.8 fm. In Table I, we have presented the calculated nuclear charge radii using RMF and E-RMF models as well as the experimental values [25], wherever available. In Table I note that both models, RMF as well as E-RMF, give similar results for nuclear radii and both account fairly well for the experimentally observed values. Because the charge radius is obtained from the density profile and our RMF and E-RMF results for r_c match excellently with experimental results, we can use these density profiles in the cross-section calculations reliably, which is the main objective of the present study.

B. Input for Glauber model

The main input required for calculating the cross sections using the Glauber model includes the target and projectile nuclear densities. The nuclear densities obtained from RMF calculations are then fitted by a sum of Gaussian functions with appropriate coefficients c_i and ranges a_i chosen for the respective nuclei as,

$$\rho(r) = \sum_{i=1}^{N} c_i \exp[-a_i r^2]. \tag{17}$$

In the present work, the RMF and E-RMF densities have been fitted with a sum of two Gaussians and the calculated coefficients c_1, c_2 and ranges a_1, a_2 are listed in Table II.

This fitting makes it possible to obtain analytic expression for the transparency functions as defined in Eqs. (10) and (12) and hence simplify further numerical calculations [26]. In Fig. 1(a), we show the total density distribution (ρ) of ^{11}Li obtained from RMF and E-RMF formalisms, using spherical coordinate basis, fitted with Eq. (17). For the same nucleus, the

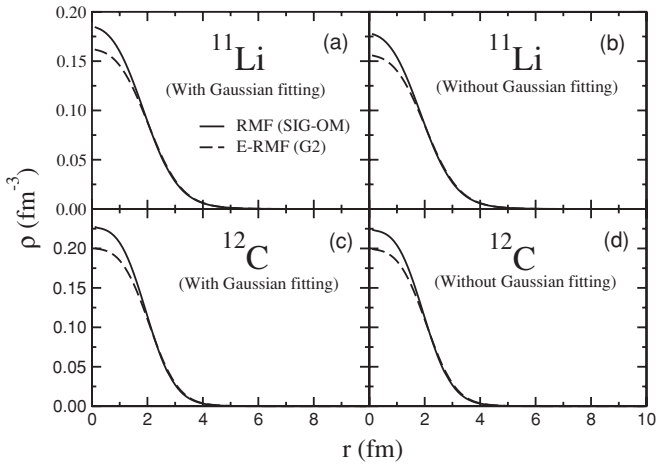

FIG. 1. Comparison of density distribution obtained from RMF and E-RMF calculations: (a) for ^{11}Li nucleus with Gaussian fitting, (b) for ^{11}Li nucleus without Gaussian fitting, (c) for ^{12}C nucleus with Gaussian fitting, and (d) for ^{12}C nucleus without Gaussian fitting.

TABLE III. The averaged nucleon-nucleon cross sections $\bar{\sigma}_{NN}$ (in fm^2) and other parameters used for calculation of profile function.

Energy (in MeV/nucleon)	30	49	85	100	120	150	200
$\bar{\sigma}_{NN}$	19.6	10.4	6.1	5.29	4.72	3.845	3.28
α_{NN}	0.87	0.94	1.0	1.435	1.38	1.245	0.93
β_{NN}	0.0	0.0	0.0	1.02	1.07	1.15	1.24
Energy (in MeV/nucleon)	325	425	500	625	800	1100	2200
$\bar{\sigma}_{NN}$	3.03	3.025	3.62	4.0	4.26	4.32	4.335
α_{NN}	0.305	0.36	0.04	−0.095	−0.07	−0.275	−0.335
β_{NN}	0.62	0.48	0.125	0.16	0.21	0.22	0.26

actual ρ (i.e., without Gaussian fitting) is shown in Fig. 1(b) for comparison. It is noticed that the results of RMF and E-RMF are quite similar except a small difference at center. Further, it has also been observed that the nuclear densities fitted by a sum of Gaussian functions are almost similar to the actual nuclear densities. We have repeated the same calculations for ^{12}C using RMF and E-RMF numerical methods and the results are plotted in Figs. 1(c) and 1(d). In this case also the results follow the same trend as in case of the ^{11}Li nucleus.

The calculation of profile function Γ requires some phenomenological parameters related to the nucleon-nucleon cross section. These parameters, $\bar{\sigma}_{NN}, \alpha$, and β, at various energies are taken from Refs. [13,22] and tabulated in Table III for the sake of completeness. Here σ_{NN} represents the total cross section of NN collisions, α_{NN} is the ratio of the real to the imaginary part of the forward nucleon-nucleon scattering amplitude, and β_{NN} is basically the slope parameter that determines the fall of the angular distribution of the NN elastic scattering. Though these parameters in general depend on the isospin of the nucleons (pp, nn, pn), appropriate average values are taken by interpolating a given set. The nucleon-nucleon cross section, $\bar{\sigma}_{NN}$, averaged over neutron and proton numbers is calculated by the expression [22,27]

$$\bar{\sigma}_{NN}(E) = \frac{N_p N_T \sigma_{nn} + Z_p Z_T \sigma_{pp} + N_p Z_T \sigma_{np} + N_T Z_p \sigma_{np}}{A_p A_T}, \tag{18}$$

where A_p, A_T, Z_p, Z_T, and N_p, N_T are the projectile and the target mass, charge, and neutron numbers, respectively.

C. Total reaction cross section

The total reaction cross sections at different incident energies have been calculated for various systems and compared with the experimental results [28], if available. The reaction cross section with stable and unstable beams using stable target such as ^{12}C are within experimental reach and are being studied extensively [29]. As a first application to nuclear reaction studies, we calculated the total reaction cross section for the ^{12}C+^{12}C system and compared it with the experimental results [10,30]. It can be seen from Fig. 2 that the agreement of σ_r using E-RMF nuclear densities is excellent for almost all incident energies (energy/nucleon), particularly at higher values. The calculated E-RMF cross section is slightly off at lower energies, which is easily understandable as it is well studied that the Glauber model works better at higher incident energies in comparison to the lower incident energies. This disagreement is due to the significant role played by the repulsive Coulomb potential whose effects are obvious in the low-energy range. Such a Coulomb effect breaks the characteristic Glauber assumption that the projectile travels along straight-line trajectories. However, our results using E-RMF nuclear densities successfully produce the qualitative trend of experimental results. Here it is interesting to see that the calculations using RMF densities also matches reasonably with the experimental values but the results at lower incident energies are quite off.

In Figs. 3 and 4, we show the comparison of experimental [1,4,5] and calculated σ_r for $^{6-11}$Li + ^{12}C, $^{7-14}$Be + ^{12}C, and $^{8-17}$B+^{12}C systems at fixed incident energy (800 MeV/nucleon). The trends of the calculations for the different projectiles (Figs. 3 and 4) are basically the same.

So far we have discussed the reactions involving stable and unstable beams on stable target. To measure the nuclear reaction cross section with an unstable beam and unstable target is one of the major challenges for experimental nuclear physicists. Such measurements would be helpful for the better

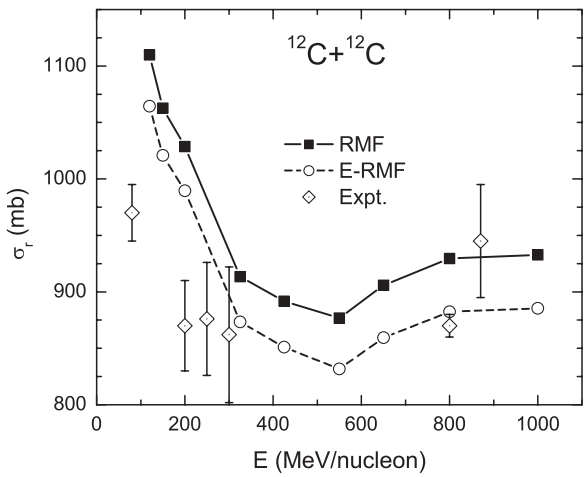

FIG. 2. The total reaction cross section (σ_r) for the ^{12}C +^{12}C system. Experimental data are also shown in the figure with error bars [10,30].

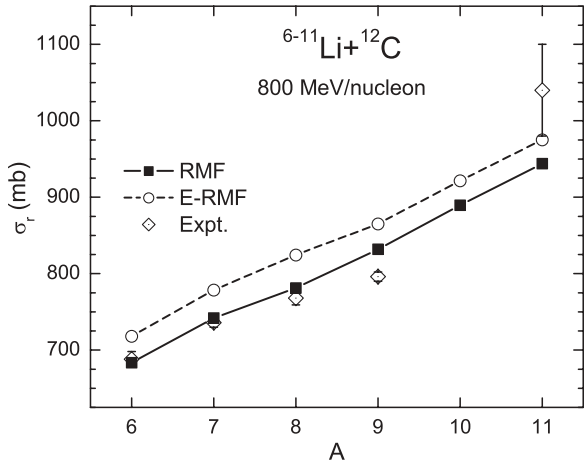

FIG. 3. The total reaction cross section (σ_r) at 800 MeV/nucleon for Li isotopes as projectile and ^{12}C as target. Experimental data with error bars [1,4,5] are also shown.

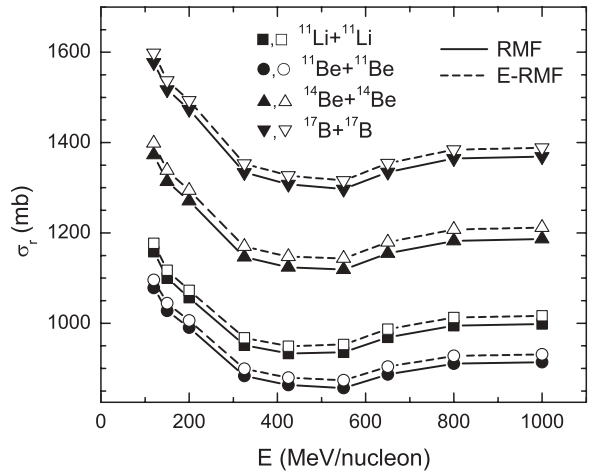

FIG. 5. Total reaction cross section for ^{11}Li+^{11}Li, ^{11}Be+^{11}Be, ^{14}Be+^{14}Be, and ^{17}B+^{17}B with RMF and E-RMF densities as input for various incident energies.

understanding of many astrophysical phenomena as well as in determining the energy and matter evolution at stellar sites. As more extensive observational data are gathered from Earth and space observatories, an ever-greater demand is placed on our knowledge of the basic physical processes that probe astrophysical phenomena. Considerable efforts at the Institute of Modern Physics, CAS (China), and at RIKEN (Japan) are underway to look for RIB+RIB cross sections using RIB as internal target with RIB projectile. Although such measurements are not feasible with presently available experimental techniques, the fast advancement in RIB techniques may provide us this facility in the next few years or so. Such experiments will be decisive in getting precise

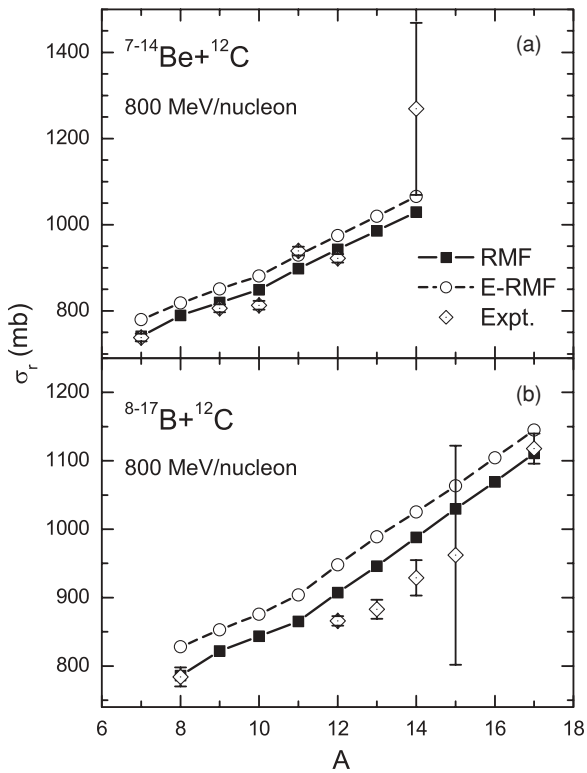

FIG. 4. (a) Same as Fig. 3, but for Be isotopes as projectile. (b) Same as Fig. 3, but for B isotopes as projectile. Experimental data are taken from Refs. [1,4,5]

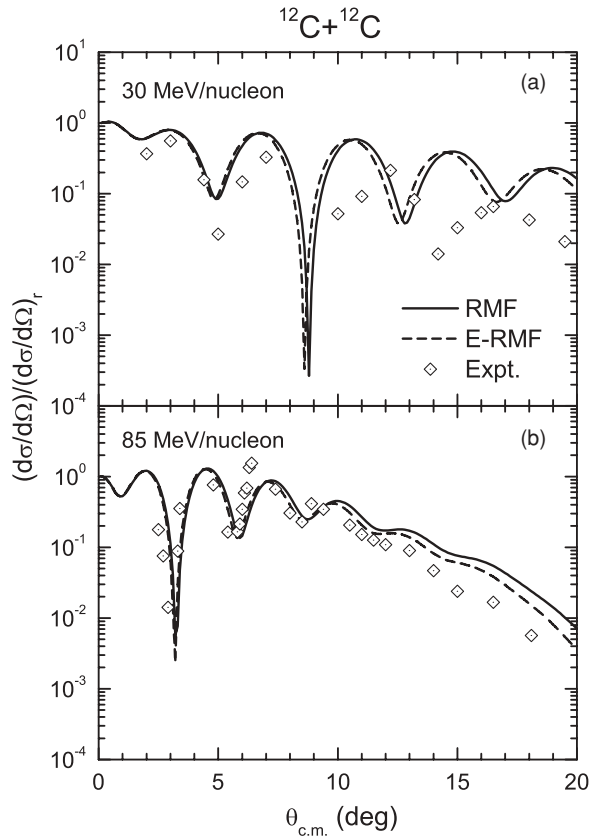

FIG. 6. Differential cross section for ^{12}C+^{12}C system: (a) at 30 MeV/nucleon of incident energy and (b) at 85 MeV/nucleon of incident energy. The experimental data are taken from Ref. [28].

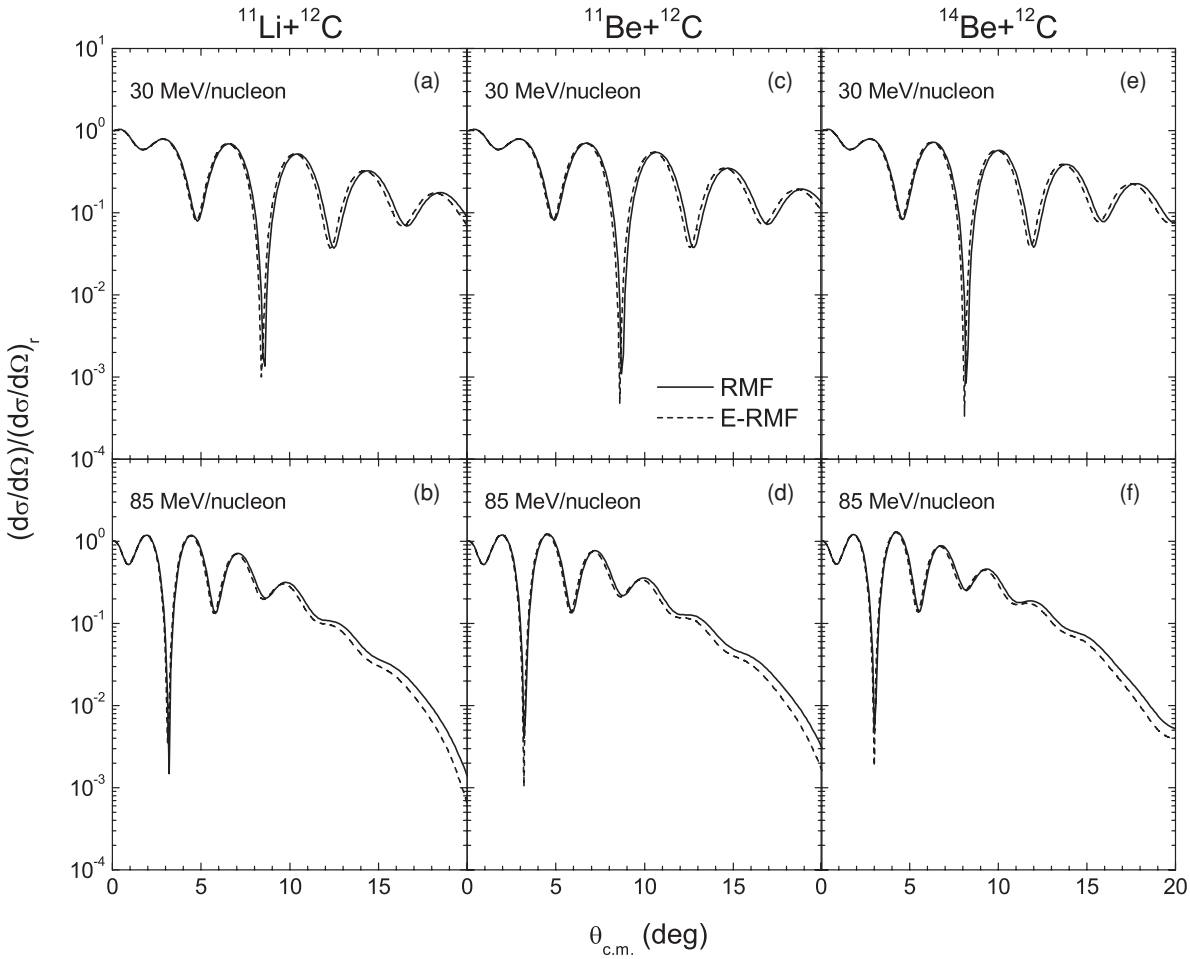

FIG. 7. Same as Fig. 6 but for ^{11}Li, ^{11}Be, and ^{14}Be as projectiles.

information about the structure of halo nuclei. In this view, we have presented the calculated σ_r for few RIB+RIB systems, namely for ^{11}Li+^{11}Li, ^{11}Be+^{11}Be, ^{14}Be+^{14}Be, and ^{17}B+^{17}B in Fig. 5, which may serve as a guiding tool for the experiments under planning. We see from Fig. 5 that RMF and E-RMF predict almost similar trend for the variation of cross section with respect to energy. A further inspection of the figure reveals that the E-RMF results are marginally higher than the RMF results.

D. Differential cross section

Results for the elastic differential cross section $(d\sigma/d\Omega)/(d\sigma/d\Omega)_r$ for the ^{12}C+^{12}C system have been shown in Fig. 6 at 30 MeV/nucleon as well as 85 MeV/nucleon of incident energies. We see that the elastic scattering angular distributions for ^{12}C+^{12}C, are better reproduced using E-RMF (G2 set) nuclear densities than RMF (SIG-OM) one while demanding conformity with experimental data [28]. This example clearly shows the importance of nuclear densities and highlights the sensitivity of the experimental differential cross section to details of nuclear structure. Results for the elastic scattering angular distributions for RIB projectiles are shown in Fig. 7.

From the above study, it is interesting to observe that the two relativistic approaches give slightly different cross sections that could be attributed to the different results obtained for ground-state properties. Hence the details of structure information have to be considered crucial as they are well reflected in the reaction cross sections. At the low-energy region (30 MeV/nucleon), both differential scattering cross sections (SIG-OM and G2) are similar to each other as shown in Fig. 6(a). The experimental trend is reproduced well using both the densities as input in the evaluation of differential cross section. However, if one analyzes the data at 85 MeV/nucleon as shown in Fig. 6(b), the values of $(d\sigma/d\Omega)/(d\sigma/d\Omega)_r$ obtained with both RMF and E-RMF approaches agree well with those of the experiment, both qualitatively and quantitatively.

Similar results of differential cross section for exotic nuclei which are predicted as likely halo candidates, namely ^{11}Li, ^{11}Be, and ^{14}Be [4], with ^{12}C as target nucleus is shown in Fig. 7 taking incident energies as 30 and 85 MeV/nucleon. In all these systems, i.e., ^{11}Li+^{12}C, ^{11}Be+^{12}C, ^{14}Be+^{12}C, the differential cross sections obtained

with both, the RMF and the E-RMF densities are almost similar.

IV. SUMMARY

In summary, we used the Glauber model to calculate nuclear reaction cross sections with densities obtained from RMF and E-RMF calculations using the SIG-OM and G2 sets of parameters, respectively. We have seen that the calculation of the total reaction cross section can be performed well with the Glauber model using RMF and E-RMF nuclear densities as the main ingredient. The good quality of results shows that the nuclear reaction cross-section predictions from the Glauber-model calculations using RMF and E-RMF nuclear densities will be helpful in more stringent analysis of the high-energy reactions involving the nuclei on either side of the valley of β stability. The comparison with the results of double folding potential analysis using the same RMF and E-RMF nuclear densities would further enrich our knowledge in this regard for the low-energy region.

While analyzing the differential cross section with the RMF and E-RMF densities, we found that both results are quite comparable to each other. However, further inspection suggests that the differential cross section obtained by the E-RMF density is closer to the experimental values than the RMF results. The RMF slightly fails for larger scattering angles with higher incident energy. Overall, these calculations give an excellent account for the existing experimental data for ground-state properties, namely nuclear radii and binding energy as well as for nuclear reaction cross-section results. Further, it is hoped that such precise studies for cross-section calculations of exotic nuclei may also be very crucial in view of upcoming radioactive ion-beam facilities.

ACKNOWLEDGMENTS

One of the authors (SKP) would like to acknowledge the financial support provided by DST, Govt. of India vide sanction No. SR/S2/HEP-16/2005.

[1] A. Ozawa, T. Suzuki, and I. Tanihata, Nucl. Phys. **A693**, 32 (2001).
[2] D. T. Khoa, H. S. Than, T. H. Nam, M. Grasso, and N. V. Giai, Phys. Rev. C **69**, 044605 (2004).
[3] F. M. Nunes, N. C. Summers, A. M. Moro, and A. M. Mukhamedzhanov, *Proceedings of Nuclei at the Limits*, ANL July 26–30, 2004; arXiv: nucl-th/0505046.
[4] I. Tanihata, J. Phys. G **22**, 157 (1996).
[5] I. Tanihata, H. Hamagaki, O. Hashimoto, Y. Shida, N. Yoshikawa, K. Sugimoto, O. Yamakawa, T. Kobayashi, and N. Takahashi, Phys. Rev. Lett. **55**, 2676 (1985).
[6] T. Kobayashi, O. Yamakawa, K. Omata, K. Sugimoto, T. Shimoda, N. Takahashi, and I. Tanihata, Phys. Rev. Lett. **60**, 2599 (1988).
[7] P. G. Hansen and B. Jonson, Europhys. Lett. **4**, 409 (1987).
[8] W. Mittig *et al*., Phys. Rev. Lett. **59**, 1889 (1987).
[9] K. Varga, S. C. Pieper, Y. Suzuki, and R. B. Wiringa, Phys. Rev. C **66**, 034611 (2002).
[10] B. Abu-Ibrahim, Y. Ogawa, Y. Suzuki, and I. Tanihata, Comput. Phys. Commun. **151**, 369 (2003).
[11] R. J. Glauber, *Lectures in Theoretical Physics*, edited by W. E. Brittin and L. G. Dunham (Interscience, New York, 1959), Vol. 1, p. 315.
[12] G. F. Bertsch, B. A. Brown, and H. Sagawa, Phys. Rev. C **39**, 1154 (1989).
[13] M. Y. H. Farag, Eur. Phys. J. A **12**, 405 (2001).
[14] A. Bhagwat and Y. K. Gambhir, Phys. Rev. C **69**, 014315 (2004); A. Bhagwat, Y. K. Gambhir, and S. H. Patil, Eur. Phys. J. A **8**, 511 (2000); J. Phys. G **27**, B1 (2001).
[15] B. K. Sharma, S. K. Patra, Raj K. Gupta, A. Shukla, P. Arumugam, P. D. Stevenson, and Walter Greiner, J. Phys. G: Nucl. Part. Phys. **32**, 2089 (2006).
[16] S. K. Patra and C. R. Praharaj, Phys. Rev. C **44**, 2552 (1991); Y. K. Gambhir, P. Ring, and A. Thimet, Ann. Phys. (NY) **198**, 132 (1990).
[17] B. D. Serot and J. D. Walecka, Int. J. Mod. Phys. E **6**, 515 (1997).
[18] R. J. Furnstahl, B. D. Serot, and H. B. Tang, Nucl. Phys. **A598**, 539 (1996); **A615**, 441 (1997).
[19] P. Arumugam, B. K. Sharma, P. K. Sahu, S. K. Patra, T. Sil, M. Centelles, and X. Viñas, Phys. Lett. **B601**, 51 (2004).
[20] M. Del Estal, M. Centelles, X. Viñas, and S. K. Patra, Phys. Rev. C **63**, 024314 (2001).
[21] M. Del Estal, M. Centelles, X. Viñas, and S. K. Patra, Phys. Rev. C **63**, 044321 (2001).
[22] P. J. Karol, Phys. Rev. C **11**, 1203 (1975).
[23] M. M. Haidari and M. M. Sharma, nucl-th/0702001.
[24] G. Audi, A. H. Wapstra, and C. Thibault, Nucl. Phys. **A729**, 337 (2003).
[25] I. Angeli, At. Data Nucl. Data Tables **87**, 185 (2004).
[26] Y. Ogawa, K. Yabana, and Y. Suzuki, Nucl. Phys. **A543**, 722 (1992).
[27] S. K. Charagi and S. K. Gupta, Phys. Rev. C **41**, 1610 (1990); S. K. Charagi, Phys. Rev. C **48**, 452 (1993).
[28] J. Chauvin, D. Lebrun, A. Lounis, and M. Buenerd, Phys. Rev. C **28**, 1970 (1983); M. Buenerd, A. Lounis, J. Chauvin, D. Lebrun, P. Martin, G. Duhamel, J. C. Gondrand, and P. D. Saintignon, Nucl. Phys. **A424**, 313 (1984); J. Y. Hostachy *et al*., Nucl. Phys. **A490**, 441 (1988).
[29] Yong-Xu Yang, Qing-Run Li, and Wei-Qin Zhao, J. Phys. G **28**, 2561 (2002).
[30] J. Jaros *et al*., Phys. Rev. C **18**, 2273 (1978).